

# ELECTRON ATTACHMENT RATES FOR PAH ANIONS IN INTERSTELLAR AND CIRCUMSTELLAR MEDIA: DEPENDENCE ON CHEMICAL PROPERTIES

F.Carelli<sup>1</sup>, T.Grassi<sup>1</sup>, and F.A. Gianturco<sup>1\*</sup>

Department of Chemistry and CISM, The University of Rome 'Sapienza', P.le Aldo Moro 5, 00185 Rome, Italy.

Received \*\*\*\*; accepted \*\*\*\*

## ABSTRACT

**Context.** The attachment of free electrons to polycondensed aromatic ring molecules (PAHs) is studied for a variety of such molecules with different numbers of condensed rings and over a broad range of electron temperatures, using a multichannel quantum approach. The calculations of the relevant cross sections are used in turn to obtain the corresponding attachment rates for each of the systems under study, and these rates are parametrized as a function of temperature using a commonly employed expression for two-body processes.

**Aims.** The scope of this work is to establish from first principles the influence of their chemical properties on the efficiency of electron-attachment process for PAHs.

**Methods.** Quantum multichannel scattering methods are employed to generate the relevant cross sections and hence the attachment rates.

**Results.** The rates obtained for the present molecules are found to markedly vary within the test ensemble of the present work and to be smaller than the values currently used for the full class of PAHs when models of their evolutions in ISM environments are employed. The effects of such differences on the evolutions of chemical networks that include both PAH and PAH- species are analysed in some details and related to previous calculations.

**Key words.** astrochemistry – ISM:molecules – ISM:evolution

## 1. Introduction

The widespread presence in the interstellar medium (ISM) of polycyclic aromatic hydrocarbons (PAHs), organic molecules made up of several aromatic rings fused together, as well as the existence in the same environments of their dehydrogenated, ionized and/or protonated counterparts, has been largely inferred from the extensive presence of unidentified infrared emission bands that have been observed in the range of 3 to 14 micrometers (D'Hendecourt & Ehrenfreund 1997; Rhee et al. 2007; Parker et al. 2012; Ricks et al. 2009). Current astrochemical models for the PAH formation have largely been derived from the combustion chemistry community that suggested how these formation processes should occur in warm and dense circumstellar envelopes of carbon-rich stars through sequential reactions of smaller radicals with acetylene at temperatures around 1000 K (Cherchneff et al. (1992) and erratum). Even more recently, their formation at temperatures down to 10 K has been surmised after an interesting investigation combining cross molecular beam studies and quantum chemistry calculations (Parker et al. 2012).

Another low-energy path to possible formations of PAHs has come from investigating the role of the free electrons which are present in the circumstellar and interstellar media and in protoplanetary atmospheres (Herbst & Osamura 2008) in order to assess from calculations and possible experimental data the likely attachment efficiency of these

free projectiles to the PAHs and the ensuing formation of very reactive anionic species, which can in turn react with radicals present in those environments (Demarais et al. 2012). That even temporary anions of smaller members of this family of aromatic molecules could be involved in subsequent reactions with cationic radicals has been suggested also in our earlier computational studies on benzyne anions (Carelli et al. 2010; Carelli et al. 2011). Recent experimental work has shown that indeed anionic PAHs like phenide ( $C_6H_5^-$ ), naphthalenide ( $C_{10}H_7^-$ ), and anthracenide ( $C_{14}H_9^-$ ) can efficiently react with H,  $H_2$  and  $D_2$  as observed in flowing afterglow-selected experiments (Demarais et al. 2012; Yang et al. 2011). It therefore follows from the above that to establish the possible effects on the chemistry of dark circumstellar regions of the presence of anionic PAHs and to model both the possible efficiency of formations and the consequences of such additional partners on the evolutionary history of that chemistry becomes of direct interest for improving our understanding of the PAH chemistry in the ISM in general. In particular, the present work wishes to analyse whether or not the chemical properties of the individual component partners in the large series of postulated PAHs play any significant role in the evolutionary studies of the chemical networks and if it is still a realistic choice to view their efficiency as given by a single rate value with a unique temperature dependence.

In the following we therefore intend to approach the problem of identifying, if at all possible, a detectable difference of behaviour, for a subset of PAHs chosen as initial examples for that entire class of molecules, which are re-

\* Corresponding author: e-mail: fa.gianturco@caspur.it Fax +39-06-49913305

lated to their differences in chemical properties. In the next section we therefore summarize the method we employ for obtaining the quantum scattering cross sections for electron collisions with the PAHs and also how we use such scattering observables to yield the relevant attachment rates. The next section III reports our results for a small group of relevant molecules and discuss their differences and relative efficiencies, while section IV describes the final effects of such differences on the evolutionary history of the chemical networks currently employed for simulations. Our present conclusions are finally given in section V.

## 2. Computing cross sections and attachment rates

### 2.1. Quantum dynamical treatment: an outline

Both the target one-electron bound orbitals and the impinging electron wavefunction are expanded as linear combination of symmetry-adapted spherical harmonics

$$\phi_i^{p\mu}(r, \theta, \phi) = \frac{1}{r} \sum_{lh} u_{lh}^{i,p\mu}(r) \chi_{lh}^{p\mu}(\theta, \phi) \quad (1)$$

where the  $\chi_{lh}^{p\mu}(\theta, \phi)$  indicate the linear combinations of spherical harmonics  $Y_l^\mu$  and the  $[p\mu]$  labels record the specific Irreducible Representation (IR) indices [13]. The assumption that the target molecule is adequately described by its ground-state Slater determinant (static exchange approximation) leads to the following simplified form for the scattering equations:

$$\left[ \frac{1}{2} \nabla^2 + (E - \epsilon) \right] F(\mathbf{r}) = \int d\mathbf{r}' V(\mathbf{r}, \mathbf{r}') F(\mathbf{r}') \quad (2)$$

that can be solved (once the model interaction potential for our system is assembled) by using the Schwinger variational method as described in our earlier publications ,e.g. see (Lucchese & Gianturco 1996). The static exchange approximation does not include the response of the target to the impinging electron, i.e. the correlation and polarization effects acting at short and at large electron-target distances respectively. That additional part of the overall interaction has been modelled in our study by writing

$$V^{cp}(\mathbf{r}) = \begin{cases} V^{corr}(\mathbf{r}) & \text{for } \mathbf{r} \leq \mathbf{r}_{\text{match}} \\ V^{pol}(\mathbf{r}) & \text{for } \mathbf{r} > \mathbf{r}_{\text{match}} \end{cases} \quad (3)$$

In the present work we have used the Lee-Yang-Parr form for  $V^{corr}(\mathbf{r})$  [15] and further employed the  $V^{pol}(\mathbf{r})$  as a function of the polarizability tensor to describe successfully, via the  $V^{cp}$  model of Eqn.(3), this additional part of the overall interaction potential. We further replace the exact nonlocal exchange interaction of Eqn.(2) with a local energy-dependent potential.

$$V_{FEGE} = \frac{2}{\pi} k_F(\mathbf{r}) \left( \frac{1}{2} + \frac{1 - \eta^2}{4\eta} \ln \left| \frac{1 + \eta}{1 - \eta} \right| \right) \quad (4)$$

where  $k_F$  is the Fermi momentum and  $\eta$  the neutral molecule ionization potential. We have already found (Lucchese & Gianturco 1996) that Eqn.(4) can yield a reasonably realistic description of such forces in a great variety of molecular systems. We can rewrite the scattering equations in homogeneous form to obtain the static-model-exchange-correlation-polarization (SMECP) approximation for the scattering event

$$\left[ -\frac{1}{2} \nabla^2 - \frac{1}{2} k^2 + \hat{V}^{st} + \hat{V}^{cp} + \hat{V}^{FEGE} \right] F(\mathbf{r}) = 0. \quad (5)$$

$V(\mathbf{r})$  is the sum of the three local potentials  $V(\mathbf{r}) = V^{st}(\mathbf{r}) + V^{cp}(\mathbf{r}) + V^{FEGE}(\mathbf{r})$ , of which  $V^{st}(\mathbf{r})$  describes the static interaction of the scattered electron with the target's nuclei and electrons,  $V^{cp}(\mathbf{r})$  contains the correlation-polarization contributions of Eqn.(3) and the  $V^{FEGE}(\mathbf{r})$  is the model exchange potential of Eqn.(4). After integrating over the angular variables, Eqn.(5) takes the form

$$\left[ \frac{d^2}{dr^2} - \frac{l(l+1)}{r^2} + k^2 \right] F_{lh}^{p\mu}(r) = 2 \sum_{l'h'} V_{lh,l'h'}^{p\mu}(r) F_{l'h'}^{p\mu}(r), \quad (6)$$

and the potential coupling elements are given by

$$\begin{aligned} V_{lh,l'h'}^{p\mu}(r) &= \langle \chi_{lh}^{p\mu}(\hat{r}) | V(\mathbf{r}) | \chi_{l'h'}^{p\mu}(\hat{r}) \rangle = \\ &= \int d\hat{r} \chi_{lh}^{p\mu}(\hat{r}) V(\mathbf{r}) \chi_{l'h'}^{p\mu}(\hat{r}). \end{aligned} \quad (7)$$

The S-matrix elements, related to the K-matrix, yield the set of partialwave phase-shifts

$$S_l = S_l(k) = e^{2i\delta_l(k)} \quad (8)$$

for all the contributing angular momenta. For a scattering process characterized by many broad and overlapping resonances, the usual Breit-Wigner formula is no longer efficient. However it is possible to extract the positions and the widths of closely spaced resonant states by using the Q-matrix formalism

$$Q(E) = i\hbar S \frac{dS^\dagger}{dE} = -i\hbar \frac{dS}{dE} S^\dagger = Q^\dagger(E). \quad (9)$$

Eigenvalues of the  $Q$  matrix are equal to the delay time of the outgoing wavepacket, as defined in (Smith 1960). For a multichannel scattering process the trace of the  $Q$  matrix is further related to the eigenphase sum  $\delta_{sum}$ :

$$2\hbar \frac{d\delta_{sum}}{dE} = \text{Tr} Q(E) \quad (10)$$

where the eigenphase sum is defined via the elements of Eqn.(8), with  $k^2 = 2E$

$$\delta_{sum} = \sum_{l=1}^{\infty} \delta_l(E). \quad (11)$$

It can be shown that the first derivative of the eigenphase sum can be recast as a sum of Lorentzian functions, each associated to a pole of the S matrix, characterized by an energy position  $\Re(E)$  and a width  $\Im(E)$ . This is the procedure we have followed to analyse the resonance regions in our present study. In the present analysis, in fact, we limit our study to considering the target molecules to remain in the equilibrium geometries of their ground electronic states.

## 2.2. Anion formation rates

The next step in the calculations involves the thermal average over the internal states of the species in the two-body (2B) reactions that will be analysed in a moment. By assuming that the free electrons have a kinetic temperature  $T_e$  and that the molecules interacting with them have an internal distribution over states which can be associated with a temperature<sup>1</sup>  $T_M$ , the existence of local thermal equilibrium (LTE) implies, given the large differences between the electron's mass and those of the molecules, that  $T_M \neq T_e = T$  (i.e. the molecules are considered as still during collisions) and that the rate of formation of molecular anions is given by

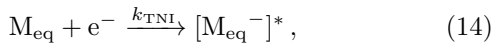
$$k_f(T) = \frac{1}{Q_v Q_r Q_{el}} \sum_n e^{-\epsilon/k_B T} \int v \sigma_n(v) f(v, T) dv, \quad (12)$$

where  $\sigma_n(v)$ , a function of the relative velocity, is the integral cross-section (ICS) for electron-molecule collision labelled by  $n$ , a global index that specifies the electronic, vibrational and rotational initial molecular states and the  $Q$ 's are their corresponding partition functions. In the present study we limit the target description to be sufficient to generate ICS which are summed over all final rotational states accessible at the considered energy (and averaged over all initial states as taken to be  $|j_0\rangle = 0$ ). The molecule is also kept in its vibrational and electronic ground states given the likely conditions in the ISM environment. If the  $f(v, T)$  is taken to be the standard Maxwell-Boltzmann electron's velocity distribution, then we can write

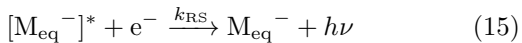
$$k_f(T) = \left( \frac{8k_B T_e}{\pi \mu_e} \right)^{1/2} \frac{1}{(k_B T_e)^2} \int E \sigma_0(E) e^{-E/k_B T} dE, \quad (13)$$

which describes the rate of anionic formation via 2B processes and with molecules in their ground electronic, rovibrational states.

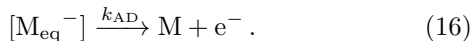
The actual molecular processes which are possible via binary collisions, could be more specifically described as those leading first to anionic metastable species formation before energy redistribution, i.e. leading to transient negative ion (TNI) formation



which corresponds, at specific energy windows, to a resonant process of attachment before molecular relaxation into a bound anion  $M^-$ . The dynamical channels of that collision process also involve direct scattering event occurring over the whole energy range. The competing processes following Eqn.(14) are given by: (i) radiative stabilization (RS) dynamics in the chiefly collisionless ISM environment



and (ii) the autodetachment (AD) process before anionic stabilization



Current assumptions consider  $k_{AD} \gg k_{RS}$  (Herbst 1981), which allows us to simplify the expression for the overall formation rate  $k_f(T)$  of Eqn.(13)

$$k_f(T) = \left( \frac{k_{TNI} k_{RS}}{k_{AD} + k_{RS}} \right) \quad (17)$$

**Table 1.** Fit coefficients for the molecules presented in this paper, where  $\alpha$  is in  $\text{cm}^3 \text{s}^{-1}$ ,  $\beta$  is dimensionless, and  $\gamma$  in K. See text and Eqn.(20) for further details.

	$\alpha$	$\beta$	$\gamma$
$\text{C}_6\text{H}_4$	10.02	-0.33	6.69
$\text{C}_6\text{H}_5$	1.44	-0.12	-14.77
$\text{C}_{14}\text{H}_{10}$	1.31	0.21	-1.12
$\text{C}_{20}\text{H}_{12}$	3.06	-0.01	2.77
$\text{C}_{24}\text{H}_{12}$	2.74	0.11	-1.12

into the form

$$k_f(T) = \left( \frac{k_{TNI}}{k_{AD}} \right) k_{RS}. \quad (18)$$

The above relation then tells us that the  $k_{TNI}$  rates can provide an **upper** bound to the true  $k_f(T)$  insofar as the radiative stabilization remains less efficient than the autodetachment process, so that we can safely assume that

$$k_f(T) \leq k_{TNI}(T), \quad (19)$$

which indicates that the calculations of  $\sigma_0(T)$  in Eqn.(13) could be approximated by evaluating the whole range of elastic ICS plus contributions to TNIs formation at specific energy windows. The latter set of cross sections have been computed in the present study and will serve us as an estimate of the anionic formation rates for PAHs in the circumstellar environments.

## 3. The computed attachment rates

In the present, exploratory, analysis we have considered a series of molecules which can help us to establish the extent of chemical diversity existing among possible PAH candidates. In particular, we have chosen two single-ring species: benzyne ( $\text{C}_6\text{H}_4$ ) and phenil ( $\text{C}_6\text{H}_5$ ) because of their having a permanent dipole moment. Thus, although they are often considered precursors molecules to the PAHs (Weaver et al. 2007), we analyse here their rates chiefly to test the relevance of their being polar molecular targets.

As examples of polyconjugated systems, we report here the attachment rates computed for anthracene (three rings:  $\text{C}_{14}\text{H}_{10}$ ), perylene (five rings:  $\text{C}_{20}\text{H}_{12}$ ), and coronene (seven rings:  $\text{C}_{24}\text{H}_{12}$ ). The full details of the cross section calculations have been already published for the coronene (Carelli et al. 2011), and are in course of publication for anthracene (Sanz et al. 2012) and perylene (Carelli & Gianturco 2012a). For the single-ring molecules, the benzyne data have already been published (Carelli et al. 2010) while the phenil cross-sections are being prepared for publication (Carelli & Gianturco 2012b). All the calculations have followed the computational method described briefly in the previous Section 2.

For the 2B reactions, the expression for the rate coefficient is usually - e.g. see Woodall et al. (2007) - written down in the following form

$$k_f = \alpha \left( \frac{T}{300 \text{ K}} \right)^\beta \exp(-\gamma/T) \text{ cm}^3 \text{s}^{-1} \quad (20)$$

so that the necessary information for a specific reaction is stored in the  $(\alpha, \beta, \gamma)$  set of parameters identifying the temperature dependence of its rate coefficient.

<sup>1</sup> Not to be confused with the kinetic molecular temperature.

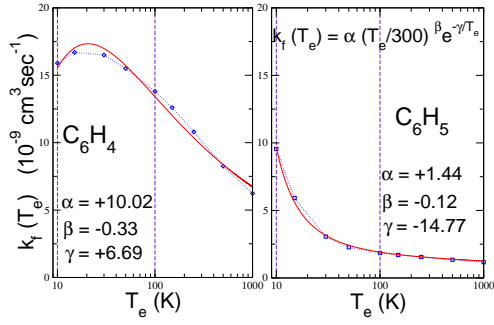


**Fig. 1.** Computed electron capture rates for phenyl and benzyne polar aromatic molecules. The corresponding fitting parameters for Eqn.(20) are also given in the Figure.

The calculations of Fig.1 report, as specific examples, the electron-attachment rates for phenyl and benzyne, over a significant range of temperatures: the parameters from the fitting suggested by Eqn.(20) are also given for each system (see Tab.1).

The calculated dipole moment of  $C_6H_4$  is 1.38 D (Kraka & Cremer 1993), while the one of  $C_6H_5$  is 0.9 D (McMahon et al. 2003); all the remaining polycondensed examples of the present work have no dipole moment. What one clearly sees from the data of Fig.1 is the strong increase of both rates at the threshold temperatures: both polar targets indicate more efficient attachment for very slow electrons, since both systems have been shown to form virtual states at zero energy and also dipole-bound states for the extra electron attached at very low collision energy (Carelli & Gianturco 2012b). Furthermore, we see that the rates for such PAH precursors vary markedly among themselves and follow the size of the permanent dipole. The latter is larger for benzyne and thus the corresponding rates for this molecule are a factor of two larger than those for phenyl at the energy thresholds. Both rates turn out to be of the order of  $10^{-8} \text{ cm}^3 \text{ s}^{-1}$  in the range of temperatures of relevance for ISM conditions (i.e. up to about 100 K), although we see that they exhibit differences in their  $T$ -dependence parameters that are sufficiently noticeable to suggest that to use a single choice of a rate for both of them would not be accurate enough. In any event, both polar molecules indicate strong increases at vanishing energies for the existence of enhanced cross section in that range of collision energies due to the presence of scattering from a dipole potential.

The situation changes quite markedly when we now move to the examples of the polycyclic hydrocarbons without permanent dipoles which are presented by the rates of Fig.2.

The following comments could be made from the data reported in the Figure:

- (i) all three examples show a different temperature dependence from those shown in Fig.1, since we now see that the rates are smallest at vanishing energies and increase with increasing  $T$ .
- (ii) the sizes of all cross-sections are around  $10^{-9} \text{ cm}^3 \text{ s}^{-1}$ , i.e. much smaller than those for polar molecules even if the number of C atoms is now larger;
- (iii) the fitting parameters change along the series but the  $\alpha$  value, somewhat proportional to the rate size, does not

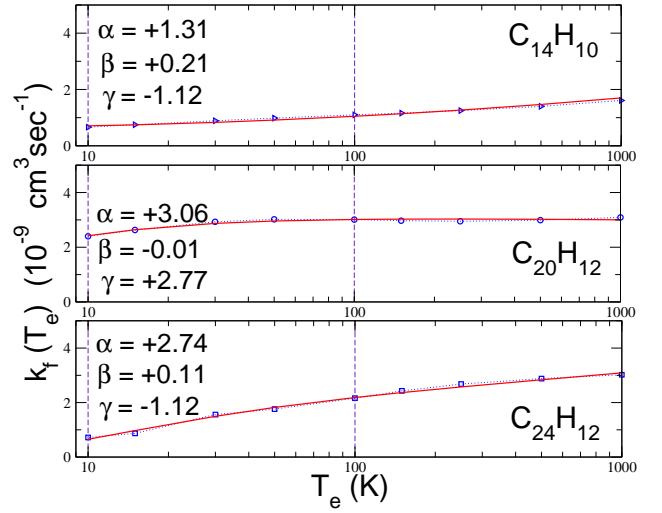


**Fig. 2.** Computed rates of electron attachment to three different polycondensed aromatic ring molecules. Top panel: anthracene; middle panel: perylene; bottom panel: coronene. See main text for further details.

increase with increasing the number of C atoms: all the cross sections are fairly similar in size and behaviour along the small series of PAHs shown in the Figure.

The present calculations seem to indicate that the chemical features of the involved PAHs do bear on the efficiency of the electron attachment rates obtained from the modelling that we have reported in the present work. The presence of a permanent dipole moment, in fact, is a significant rate-enhancer, especially at the lower temperatures, where non-polar PAHs are found to have much smaller rates. Furthermore, we see that all our computed rates, although considered to be upper bound to the true rates for such systems, are consistently smaller than the estimates employed in earlier work for such quantities (Wakelam & Herbst 2008).

It is therefore interesting to see what would be the effect of the present results on the gas-phase models for the chemistry of dense interstellar clouds which can now employ attachment rates from *ab initio* calculations. This is the aspect of the present work that we shall discuss in the following Section.

#### 4. Testing the evolutionary models

To now assess the effects of the new rates for the electron attachment processes on different PAHs on the evolution of the corresponding abundances in the ISM environments we have implemented a pseudo time-dependent dense cloud model based on the work of Wakelam & Herbst (2008) following their parameters and their recommendations for all the other rates involved in the fuller chemical network. We discuss below the comparison between the results for the overall chemical evolutions using the single value of the rate coefficient that they assume for the PAH electron attachment process (Wakelam & Herbst 2008), and the results obtained by employing the three rates proposed in this paper and individually obtained via *ab initio* calculations that we discussed in the previous sections.

For the rate coefficient  $k_{\text{EA}}$  WH2008 suggest two values already found in literature that are  $k_{fo} = 10^{-7}(N_C)^{3/4} \text{ cm}^3/\text{s}$  (Omout 1986) and  $k_{fa} = 1.2 \times 10^{-7}(N_C)^{1/2} \text{ cm}^3/\text{s}$  (Allamandola et al. 1989), where in both cases  $N_C$  is the number of carbon atoms that form the PAH. For their model they assume  $N_C = 30$  and arbitrarily decide to use the first formula as indicated in Le Page et al. (2001).

What we are therefore presenting below is a test aimed at determining the influence of using more chemically accurate electron attachment rate coefficients on the evolution of the ISM model we have employed. In particular, we track the evolution of the ISM (i) first with the aforementioned  $k_{fo}$  rate coefficient and then with the same set of other rates but changing that of the PAHs for (ii) anthracene  $k_{fA}$ , (iii) perylene  $k_{fP}$ , and (iv) coronene  $k_{fC}$ . All the other model parameters we adopt are the same as those of WH2008, namely  $n_{\text{H}_2} = 10^4 \text{ cm}^{-3}$ , a gas temperature of  $T = 10 \text{ K}$ , a cosmic-ray ionization rate of  $\zeta_{\text{CR}} = 1.3 \times 10^{-17}$ , a visual extinction  $A_v = 10 \text{ s}^{-1}$ , a PAH fractional abundance of  $3.07 \times 10^{-7}$ , and an average PAH size of  $4 \text{ \AA}$ . We have selected to show the calculations for the initial species abundances given by the model EA2 (see Tab.1 in WH2008) which is an high-metallicity scenario based on the observations of the dense cloud  $\zeta$  Ophiuchi, except for He which is set to  $n_{\text{He}} = 0.09$  compared to the total hydrogen abundance. More details of the full choice of parameters can be found in WH2008.

The results of our simulations are displayed in Fig.3 and Fig.4. The first one describes the evolution of the ionization fraction as the sum of the number densities of the negative species at a given time. WH2008 had shown a fast decrease of the total negative charge until it reaches a steady-state after  $10^3 \text{ yr}$ , while the present models have a slower decrease in time and reach the steady-state over a much longer time scale, i.e. in  $10^6 \text{ yr}$  or more. The effect of the new calculations is also shown in the figure and is rather clear: in the present model the PAHs manage to “soak” and capture much fewer electrons when compared to the results from Wakelam & Herbst (2008), since their selected single value for the attachment rate coefficient is much larger and thus indicate a more effective process. The  $\text{PAH}^-$  formed in this process rapidly recombine with the ions, thereby obtaining a more neutral gas as shown in Fig.3. On the other hand, when we replace the WH2008 rate coefficient with our separate rates for different molecules we find that the neutralization effect is less important, thus obtaining a less neutral gas once the steady-state is reached.

In a similar fashion, the data in Fig.4 show the evolution of the PAH abundances over the time range  $t = [10^2, 10^5] \text{ yr}$  and, even in this case, the effect of the new rate coefficients is evident. We obtain a larger separation between the abundances of PAH and  $\text{PAH}^-$ , a quantity that obviously increases when the attachment rate coefficients decrease with respect to the single value chosen in Wakelam & Herbst (2008).

## 5. Conclusions

In the present work we have endeavoured to analyse in some detail how one can realistically generate electron-attachment cross sections over a broad range of energies for gas-phase polycondensed aromatic molecules, a specific subset of such molecules chosen to be representative of the

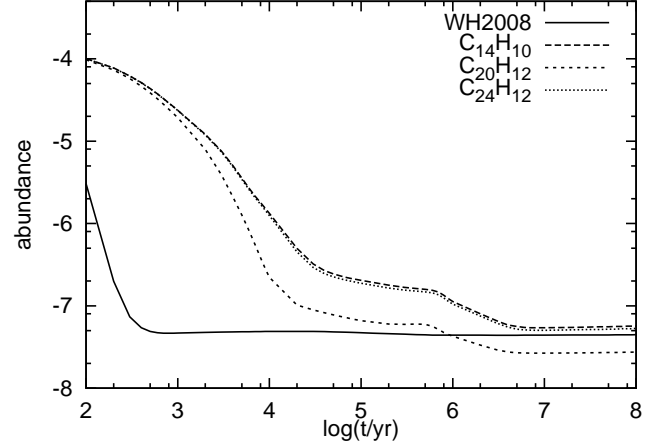


**Fig. 3.** The evolution of the total abundances of the negative charged species with time normalized to the total hydrogen number density (i.e.  $2 \times 10^4 \text{ cm}^{-3}$ ). We compare the rates from the original WH2008 model that use their selection of  $k_f$  electron attachment rates (solid) with the cases in which use instead: the anthracene rate (long-dashed), the perylene rate (dashed), and the coronene rate (dotted). See text for further details.

more general behaviour of PAHs in the interstellar and circumstellar environments. In particular, we have selected a dynamical model that employs the above cross sections to obtain attachment rates over a range of temperatures which are of direct interest in the ISM environments. The corresponding rates are essentially considered to be upper bounds to the true attachment rates, but are nevertheless found to be already larger than those employed in current evolutionary models - e.g. see Wakelam & Herbst (2008).

Furthermore, the parametric representation of computed rates is chosen to be the one usually employed in the literature to describe 2B processes in the ISM (Woodall et al. 2007) and is found by our present work to be markedly dependent on at least two chemical properties of the aromatic molecules: (i) the presence of a permanent dipole moment, a features which increases the size of the attachment rates, especially at the threshold temperatures, and (ii) only very slowly on the number of C atoms or on the number of condensed rings in the molecular system.

The captured rates have been further employed to model the time evolution within a pseudo time-dependent dense cloud description that follows the one given earlier by Wakelam & Herbst (2008). In particular, we have tried to analyse the effects of the attachment rate values produced by the present work on the evolutions of negative charged species with time (e.g. see Fig.3) and the evolutions of PAH/ $\text{PAH}^-$  abundances along the same model, as well as the electron number density changes over the same time period (see Fig.4).

The corresponding calculations suggest rather clearly that:

- (i) the attachment rates are smaller, at least over the relevant range of temperatures, than the values previously employed;

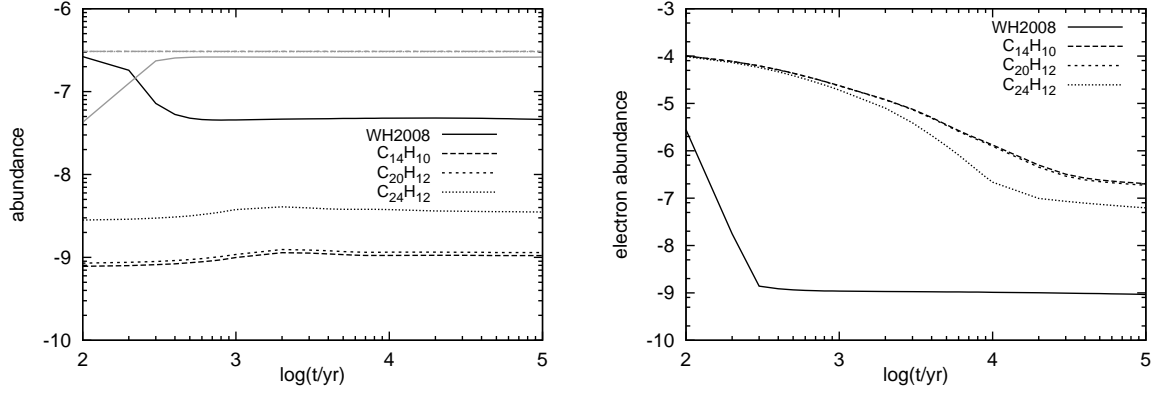


**Fig. 4.** Left panel: time evolution of the abundances of PAH (grey) and PAH<sup>-</sup> (black) normalized to the total hydrogen number density (i.e.  $2 \times 10^4 \text{ cm}^{-3}$ ). We compare the WH2008 electron attachment rates (solid) with those obtained using instead: the anthracene rates (long-dashed), the perylene rates (dashed), and the coronene rate (dotted). Note that the lines that represent the PAH densities overlap with one another, except those from WH2008. Right panel: electron number density time evolution as given by the same set of models. Note that the two panels have different vertical scales.

- (ii) they depend on the chemical properties of the specific PAH being considered, especially when comparing anthracene and coronene;
- (iii) the electron densities remain larger over a much broader range of time and reach a steady state much later than thought before (Wakelam & Herbst 2008);
- (iv) the “soaking-up” power of PAHs we have considered here turns out to be smaller than expected, hence reducing the efficiency of the neutralization processes.

Although we feel that further numerical experiments are needed in order to also include directly the efficiency of polar PAHs within the evolutionary model, the set of exemplary molecules presented here are already making clear to us that chemical variety plays a role which is bigger than previously expected and that a molecule-specific modelling of the role of electrons in evolutionary studies should be sought as much as possible.

*Acknowledgements.* The computational support from the CASPUR Consortium is gratefully acknowledged, as well as the financial support from the PRIN 2009 research network. One of us (T.G.) thanks the CINECA Consortium for the awarding of a postdoctoral grant during which this work was carried out.

## References

- Allamandola, L. J., Tielens, A. G. G. M., & Barker, J. R. 1989, *ApJS*, 71, 733  
 Carelli, F. & Gianturco, F. A. 2012a, to be submitted  
 Carelli, F. & Gianturco, F. A. 2012b, to be submitted  
 Carelli, F., Sebastianelli, F., Baccarelli, I., & Gianturco, F. A. 2010, *ApJ*, 712, 445  
 Carelli, F., Sebastianelli, F., Satta, M., & Gianturco, F. A. 2011, *Monthly Notices of the Royal Astronomical Society*, 415, 425  
 Cherchneff, I., Barker, J. R., & Tielens, A. G. G. M. 1992, *ApJ*, 401, 269  
 Demarais, N. J., Yang, Z., Martinez, O., et al. 2012, *ApJ*, 746, 32  
 D’Hendecourt, L. & Ehrenfreund, P. 1997, *Advances in Space Research*, 19, 1023  
 Herbst, E. 1981, *Nature*, 289, 656  
 Herbst, E. & Osamura, Y. 2008, *ApJ*, 679, 1670  
 Kraka, E. & Cremer, D. 1993, *Chemical Physics Letters*, 216, 333  
 Le Page, V., Snow, T. P., & Bierbaum, V. M. 2001, *ApJS*, 132, 233  
 Lucchese, R. R. & Gianturco, F. A. 1996, *International Reviews in Physical Chemistry*, 15, 429

- McMahon, R. J., McCarthy, M. C., Gottlieb, C. A., et al. 2003, *ApJ*, 590, L61  
 Omont, A. 1986, *A&A*, 164, 159  
 Parker, D. S. N., Zhang, F., Kim, Y. S., et al. 2012, *Proceedings of the National Academy of Sciences*, 109, 53  
 Rhee, Y. M., Lee, T. J., Gudipati, M. S., Allamandola, L. J., & Head-Gordon, M. 2007, *Proceedings of the National Academy of Science*, 104, 5274  
 Ricks, A. M., Doublerly, G. E., & Duncan, M. A. 2009, *ApJ*, 702, 301  
 Sanz, A. G., Carelli, F., & Gianturco, F. A. 2012, to be submitted  
 Smith, F. T. 1960, *Phys. Rev.*, 118, 349  
 Wakelam, V. & Herbst, E. 2008, *ApJ*, 680, 371  
 Weaver, S. L. W., Remijan, A. J., McMahon, R. J., & McCall, B. J. 2007, *ApJ*, 671, L153  
 Woodall, J., Agúndez, M., Markwick-Kemper, A. J., & Millar, T. J. 2007, *A&A*, 466, 1197  
 Yang, Z., Cole, C. A., Martinez, Jr., O., et al. 2011, *ApJ*, 739, 19